Assessing hydrofacies and hydraulic properties of basaltic aquifers derived from geophysical logging

Juan Navarro[1] , Elias Hideo Teramoto[1]* , Bruno Zanon Engelbrecht[1] , Chang Hung Kiang[1]

Abstract

Basaltic aquifers are an important source of water supply in many regions worldwide. Because of their cooling process, flood basalts normally have complex internal structures and unpredictable permeable zone distribution. Geophysical profiling is a reliable tool used to identify the vertical variations of physical properties within the flood basalts, mainly to distinguish between low and high permeability intervals. In this study, a detailed analysis of drill cuttings, and geophysical logging of two depth wells helped to identify the typical response of main facies of flood basalts in the Serra Geral aquifer system. The evidence obtained from this work confirms that flood basalts may be classified as multilayer aquifer systems in which a highly permeable top covers a center with low permeability as a result of recurrent floods. In several cases, permeable layers are represented by a weathering horizon developed between two flood events. This study uses an empirical model to estimate the porosity based on acoustic velocity logging. A useful model based on a well-established Kozeny-Carman model was developed to predict the permeability of basaltic rocks using porosity data. The results obtained allow to identify the permeable intervals of basaltic aquifers and to estimate their hydraulic properties.

KEYWORDS: flood basalts; geophysical logging; basaltic aquifers; Serra Geral Aquifer.

INTRODUCTION

Basaltic aquifers represent an important source of water, mainly for agricultural purposes, in many regions worldwide such as western India (Limaye 2010), the northwestern United States (Piersol and Sprenke 2015), Mexico City (Edmunds *et al.* 2002), northeastern Australia (Locsey and Cox 2003), and southern Ethiopia (McKenzie *et al.* 2001). Moreover, groundwater obtained from basalts represents the main source of water supply in volcanic islands such as Jeju Island, Korea (El-Kadi *et al.* 2014), the Canary Islands, Spain (Cabrera and Custodio 2004), Madeira Island, Portugal (Prada *et al.* 2005), and Hawaii, the United States (Wentworth 1951). Despite their importance, the distribution of permeable zones within flood basalts is poorly understood due to the internal complexity of these aquifers.

The distribution of permeable zones within basalts is intrinsically related to the internal structure of basalts that were generated by the cooling processes after a magma flood. The cooling structures have been exhaustively investigated in several studies such as those by James (1920), Tomkeieff (1940), Walker (1971), Long and Wood (1986), Lore *et al.* (2000), Kattenhorn and Schaefer (2008), Browning *et al.* (2016), and Puffer *et al.* (2018). The cooling structures create internal layers in response to distinct cooling rates within the flood, as described in Uhl and Joshi (1986), Whitehead (1992), Kulkarni *et al.* (2000), and McGrail *et al.* (2006). According to these studies, basalts typically display the same facies succession, consisting of three distinct units: flow top, flow interior, and flow bottom.

Flow tops (hereafter referred to as porous flow tops) are usually characterized by a genetic relationship between degassing, thermal contractions, and interactions with water. The tops of flood basalts are comprised of a chilled, glassy crust that is often vesicular to scoriaceous or brecciated rubble produced by escaping gas during the cooling process (Buckley and Oliver 1990, Whitehead 1992, McGrail *et al.* 2006, Zakharova *et al.* 2012). The vesicles represent the primary porosity of the rock and are generated from gas flows during lava flooding. The porosity is dependent on bubble gas and lava flow characteristics (Sahagian *et al.* 1989, Mangan and Cashman 1996, Melnik 2000) and can vary widely, as demonstrated through several experimental studies. Another characteristic identified by Buckley and Oliver (1990) described the flow top in the Deccan traps as soft and weathered, consisting of a horizon composed of green, grey, or red clay with amygdaloidal material, with a typical thickness of 1.5–3.0 m. McGrail *et al.* (2006) presented evidence of a high-lateral continuity of vesicular layers that serve as regional aquifer systems. The slow cooling within the flooded lava allows massive basalts to crystalize and become very thick. During the cooling process, contraction stress breaks the rock, generating typical colonnade and entablature structures. Long and Wood (1986) describe the colonnade as columnar structures oriented perpendicularly to flow boundaries, and typically occurring in the basal

[1]Universidade Estadual "Júlio de Mesquita Filho" – Rio Claro (SP), Brazil. E-mails: j.navarro@unesp.br, elias.hideo-teramoto@unesp.br, bruno.engelbrecht@unesp.br, chang.hung-kiang@unesp.br

*Corresponding author.

portion of the flow, alternating with entablatures. Similar to flow top, the flow bottom is comprised of a glassy, vesicular zone (*e.g.*, Whitehead 1992, Uhl and Joshi 1986, Buckley and Oliver 1990, Zakharova *et al.* 2012). However, as noted by Buckley and Oliver (1990), this zone is typically only a few centimeters thick.

The facies that comprise basalt floods present strong variations of physical properties (*e.g.*, Peterson and Lao 1970, Helm-Clark *et al.* 2004, Asfahani *et al.* 2011, Zakharova *et al.* 2012). The strong contrast in physical properties means that geophysical logging is a prominent tool that can be used to characterize the stratigraphic features of flood basalts (Helm-Clark *et al.* 2004). An extensive revision of geophysical logging was described in detail by Helm-Clark *et al.* (2004), while Zakharova *et al.* (2012) analyzed the hydraulics of core samples and geophysical logging data from basalt formations of the Columbia River Basalt Group. The porosity, represented by vesicles and fractures, is one of the main features that govern the variation of physical properties of basalts, as demonstrated by several authors such as Helm-Clark *et al.* (2004), Asfahani (2011), and Zakharova *et al.* (2012).

Despite their global abundance and importance, research on basaltic aquifers is less common when compared to typical granular aquifers. Since basalt acts as an important reservoir, this study aims to identify the parameters derived from geophysical logging that allow us to diagnose the facies variation within flood basalts. Furthermore, this research aims to develop empirical models that produce reliable estimates of porosity and permeability of rocks using geophysical logging.

METHODOLOGY

Study area

The Serra Geral formation represents one of the largest continental flood basalt occurrences, covering nearly 917,000 km^2 (Frank *et al.* 2009). According to Almeida (1986), the Serra Geral formation represents a thick sequence flow of mainly basaltic rocks, with a maximum thickness of 1,700 m, belonging to the continental-scale Paraná-Etendeka Magmatic Province. According to Turner *et al.* (1994), the age of magmatism ranges from 137 to 127 Ma. The stratigraphy, geochemistry, and tectonic history of Serra Geral were exhaustively studied in works including Frank *et al.* (2009), Machado *et al.* (2015), Barreto *et al.* (2016), Polo *et al.* (2018), Rossetti *et al.* (2018), and Svensen *et al.* (2017).

Wireline logs for the open section of two boreholes (340–1,250 m) were acquired in the county of Colômbia, São Paulo State, located in the southeast region of Brazil (Fig. 1). The analyzed basalt was covered by sandstone and claystone, belonging to the Bauru Group of the Cretaceous age, that were nearly 100 meters thick. The basalt also covers the sandstone of the Pirambóia and Botucatu formations.

Geophysical profile analysis

Based on descriptions provided in previous works, flow tops were interpreted as permeable zones, characterized by low resistivity, low sonic velocity, and high gamma rays. Using this log analysis coupled with rock samples, the typical basalt succession found is comprised of low permeability levels being vertically succeeded by high permeability horizons. The large intervals of geophysical profiling provide the possibility of identifying the limits of flood basalts and the proportion of permeable layers within the individual flood basalt flows. The wireline logs were conducted prior to well completion. Caliper (borehole diameter), total natural gamma radioactivity, electrical resistivity, and sonic velocities data were acquired using Schlumberger profiling tools. The drill cuttings description was also employed during well logs interpretation. Our analysis was restricted to total natural gamma radioactivity, electrical resistivity, and sonic velocities, since these combined parameters sufficiently describe the variation of flood basalts' internal structures.

Resistivity and sonic logs represent the most useful methods for identifying flow tops and flow interiors because of the strong variation in porosity observed therein. According to Helm-Clark *et al.* (2004), resistivity represents the best logging method to discriminate between permeable and impermeable zones of basaltic aquifers. Basalt is one of the most resistive rocks in the Earth's crust (Helm-Clark *et al.* 2004) and the resistivity of low-porosity flow interior is markedly high. Thus, an increase of porosity and, consequently, stored water content, promote a sharp decrease in resistivity. Porosity neutrons and sonic logs are very suitable for the identification of permeable and impermeable zone limits (Buckley and Oliver 1990, Helm-Clark *et al.* 2004, Zakharova *et al.* 2012), since porosity and permeability are correlated.

The sonic P wave velocity log (Vp) corresponds to the propagation velocity of an elastic wave through the tested geological unit. Due to the differences in elastic properties in response to porosity (Zamora *et al.* 1994, Planke *et al.* 1999, Chen *et al.* 2015), Vp represents an important tool to estimate basalt porosity. Vp also allows to identify fractured zones (Schlumberger 1989) as indicated by an increase in the travel time required for the pulse to reach the detectors. Similar to the resistivity, acoustic velocity is high in the massive interior of flows, and low at flow tops and interbeds.

Natural rocks emit gamma rays in response to decay chains of radioisotopes ^{40}K, ^{238}U, and ^{232}Th and their derivative products. Thus, the gamma-ray log indirectly measures the amount of radioactive species in rocks. The gamma-ray log is normally reported in American Petroleum Institute (API) units (Schlumberger 1989). Thus, gamma-ray log is a useful tool to identify potassium-rich intervals in basalt or clay content in interbed sediments, as reported by Helm-Clark *et al.* (2004). Buckley and Oliver (1990) demonstrated that gamma-rays are also useful to identify weathered zones, where the abundance of clay minerals is noticeable.

Porosity and permeability derived from empirical models

Sonic logs are useful techniques to estimate porosity using either the Wyllie time-average equation (Wyllie *et al.* 1956) or the model proposed by Raymer *et al.* (1980). However, these equations were developed for sedimentary rocks (mainly

limestone and sandstone) and therefore have low representativeness in the estimation of basalt porosity. For a more realistic approach to quantify the porosity of basalt and to improve estimations thereof, we developed an empirical model based on sonic velocity data. To this end, experimental data relating porosity and sonic velocities in basaltic rocks, compiled from previous works (Al-Harthi *et al.* 1999; Zamora *et al.* 1994, Planke *et al.* 1999, Chen *et al.* 2015, Vedanti *et al.* 2018, Rossetti *et al.* 2019), were employed in a regression analysis. As noted by Helm-Clark *et al.* (2004), the use of neutron logs

can potentially result in porosity overestimation in the presence of hydrous minerals, making velocity logs a better approach for porosity estimation.

The Kozeny-Carman model represents a common approach for predicting the permeability of volcanic rocks using porosity data (*e.g.*, Klug and Cashman 1996, Saar and Manga 1999, Mueller *et al.* 2005, Takeuchi *et al.* 2008, Yokoyama and Takeuchi 2009, Degruyter *et al.* 2010, Farquharson *et al.* 2015, Lamur *et al.* 2017). To identify a model capable of predicting permeability from porosity, porosity and permeability measurements
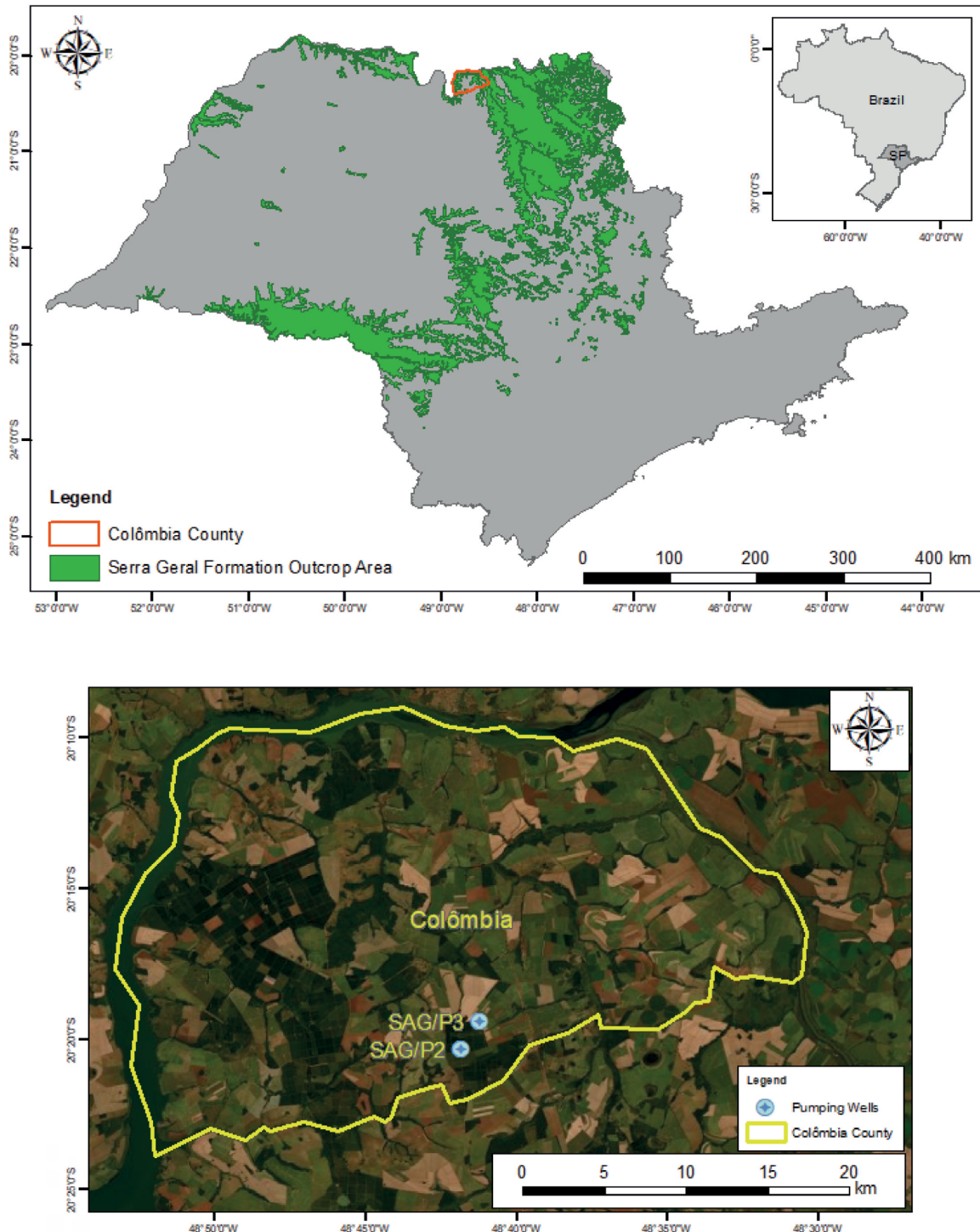

Figure 1. Location of Colômbia, where the wireline logs were acquired, and areal extension of the Serra Geral formation outcrop zone in São Paulo State.

were obtained from previous literature. Despite the abundance of experimental data related to the porosity and permeability of general volcanic rocks, our analysis was restricted to basaltic rocks, gathering 206 pieces of experimental data relating permeability and porosity, presented by Saar and Manga (1999), Mueller *et al.* (2005), Loaiza *et al.* (2012), Lamur *et al.* (2017), Rossetti *et al.* (2019), Schaefer *et al.* (2015), Bai *et al.* (2010), and Luhmann *et al.* (2017). By means of non-linear regression, we built an empirical equation to estimate permeability derived from porosity values, based on the Kozeny-Carman model.

RESULTS AND DISCUSSION

Interpretation of wireline logs

Figures 2 and 3 present the wireline logs in the open section of wells SAG/P2 and SAG/P3. The data obtained include total natural gamma radioactivity, electrical resistivity, and sonic velocities. Based on cuttings descriptions and well logs, we were able to recognize four distinct hydrofacies:

- vesicular basalt;
- massive;
- weathered basalt;
- clay lenses.

Internal structures of flood basalt

Basalts may be classified as multilayered aquifer systems, on which low-permeable levels (flow interiors) are recurrently overlapped by high-permeability zones (flow tops). This alternation of intervals is highly comparable to the genetic nature of successive covering of basaltic lava flow events. The framework of a basalt flow generated from cooling creates a vesicular and permeable zone on the flow top and a massive, entablature, or colonnade zones in the flow interior. This alternating pattern was identified in the wireline logs presented in this work and in previous ones, such as those by Buckley and Oliver (1990),
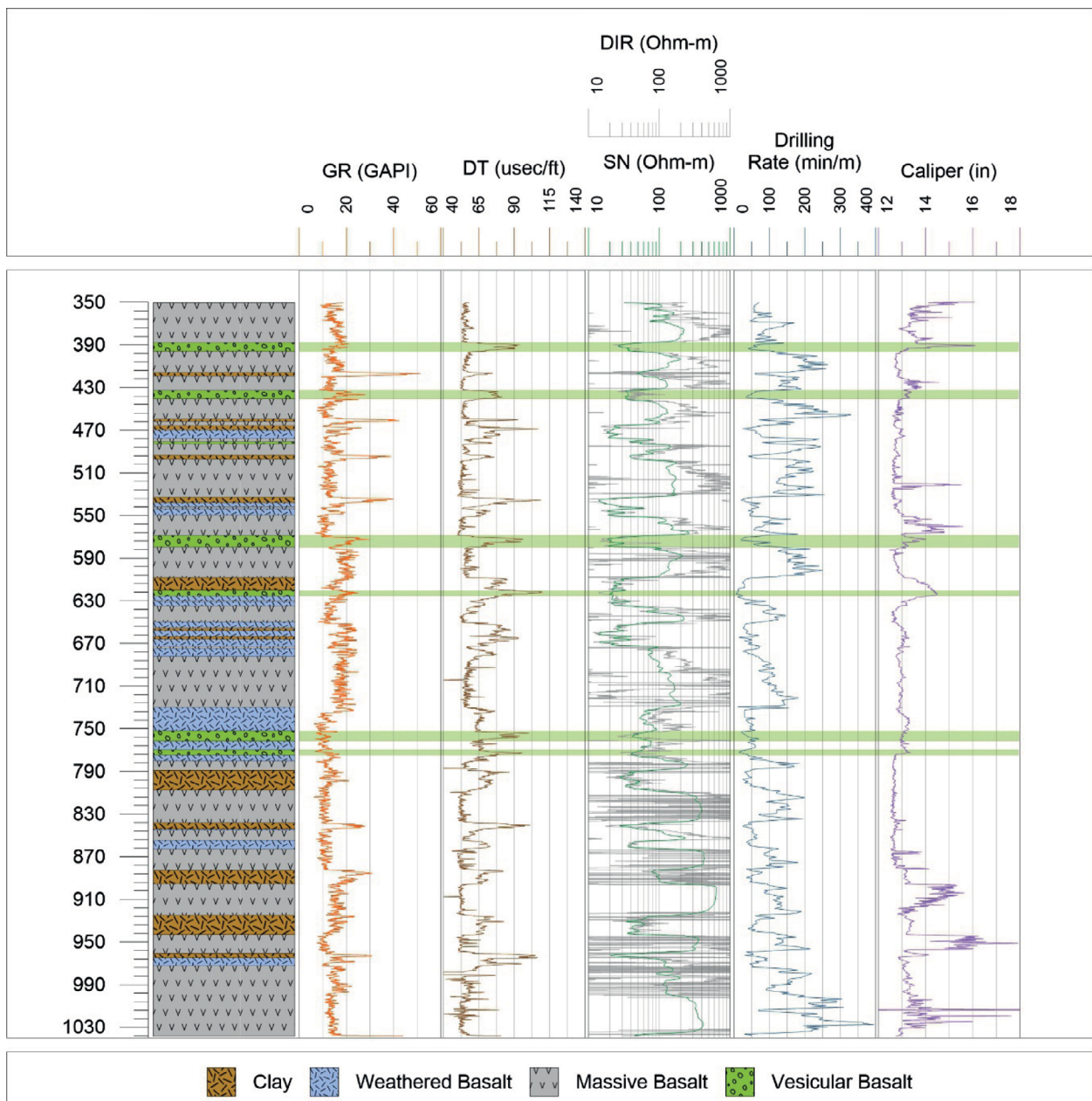

Figure 2. Geophysical logs of Well SAG/P2 in the municipality of Colombia, São Paulo, southeastern Brazil.
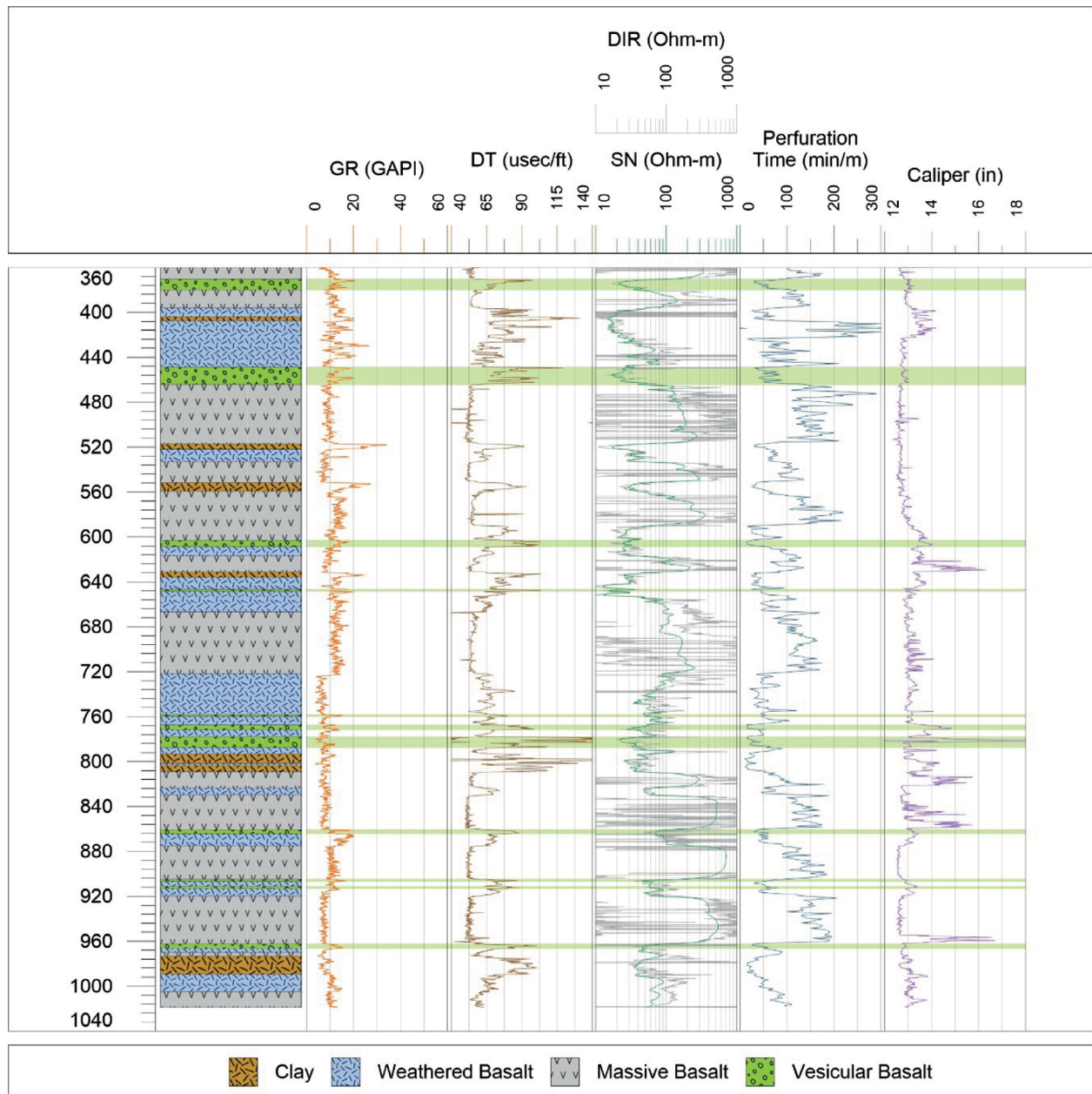
Figure 3. Geophysical logs of Well SAG/P3 in the municipality of Colombia, São Paulo, southeastern Brazil.

Crosby and Anderson (1971) Helm-Clark *et al.* (2004), Asfahani (2011), and Zakharova *et al.* (2012).

The description of drill cutting samples collected at 2 m intervals allowed us to identify 4 major facies within the drilled wells: flow interior (massive, colonnade, entablature basalts), flow tops (vesicular basalt), weathered basalt, and clay lenses. Because each facies that comprises flood basalts has a distinct range of variation in terms of density, permeability, and porosity, the responses of each geophysical method are dissimilar. Thus, the association of range values of geophysical parameters offers an unambiguous diagnostic of flood basalt internal facies. Figure 4 illustrates the boxplot of distribution of gamma-ray, electrical resistivity, and sonic P wave velocity values measured in the two wireline logs.

Flow interior

The flow interior — composed of massive basalt and/or layers of colonnade and entablature generated by slow

cooling within the center of lava flow — is characterized by low porosity and permeability and, as a result, by high resistivity (> 1,000 Ohm.m) and high Vp (mostly > 5 km/s), as seen in Figure 4. These features are unambiguously associated with massive dark gray or black basalts. A detailed description of SAG/P2 and SAG/P3 drill cuttings confirms that the electrical resistivity is the most important parameter to distinguish between high-permeability flow tops and the low-permeability flow interiors, as described by Helm-Clark *et al.* (2004).

Due to the remarkable contrast in resistivity, Helm-Clark *et al.* (2004) argue that resistivity logs represent the most useful tool to identify basalt facies, which are associated with low resistivity in interflow zones and in interbeds, and high resistivity in flow interior. Figure 4 reveals that the median resistivity of massive basalt is 563.24 $\Omega \cdot$m. Moreover, the high variability of electrical resistivity in the evaluated log, ranging from 20.6 to 100,000 $\Omega \cdot$m represents a wider range than that recorded by Zakharova *et al.* (2012) (*i.e.*, 10 to 2,000 $\Omega \cdot$m).
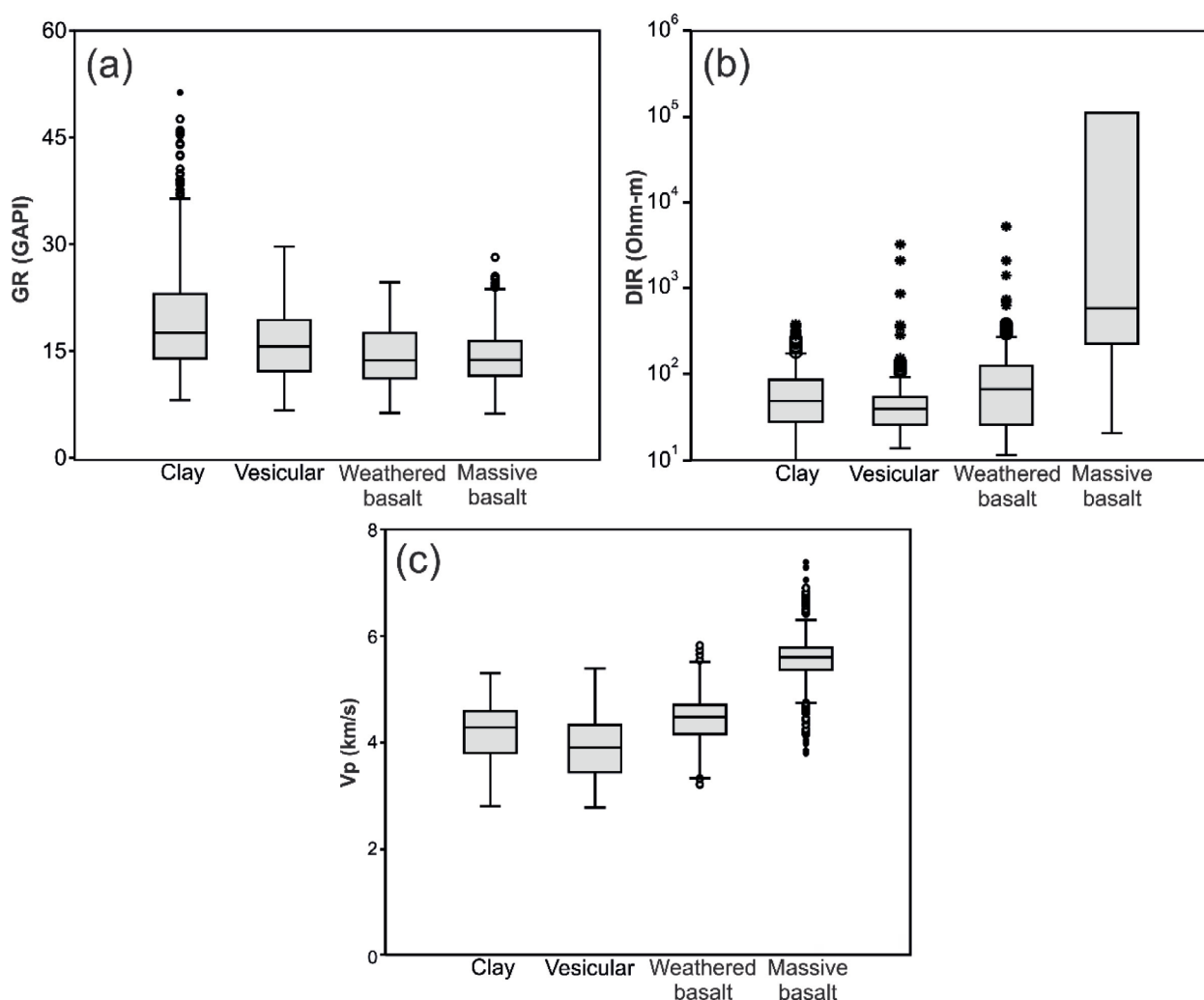
Figure 4. Boxplots showing the distribution of some wireline log parameters: (A) gamma-ray; (B) electrical resistivity; (C) sonic P wave velocity. The lower and upper caps at the end of each box indicate, respectively, the minimum and maximum values, the box limits are defined by the first and third quartiles, and the line in the center of the box represents the median.

Helm-Clark *et al.* (2004) describe that the increase in acoustic velocity is associated with massive basalt, while the decrease of acoustic velocity may be associated with sedimentary interbeds, fractured zones, or vesicular basalts. Higher Vp is directly related to both higher density and low-porosity of massive basalt. According to the experimental verification by Zamora *et al.* (1994), Al-Harthi *et al.* (1999), Planke *et al.* (1999) and others, the travel time of acoustic P wave velocity is intrinsically related to basalt porosity. The median value of Vp associated with flow interior is 5.6 km/s (Fig. 4), noticeably above the values of vesicular, weathered, and clay horizons. The range of sonic velocities observed from massive basalts in the present study (4.03–5.98 km/s) is similar to that presented by Zakharova *et al.* (2012) in the Columbia River Basalt Group (CRBG).

Vesicular basalt

Contrary to flow interior, the vesicular basalt is notably marked by its rapid cooling. The escape of bubble gas during cooling creates a network of interconnected pores. As illustrated in Figures 2 and 3, the vesicular zones comprise a limited proportion of a basalt flow.

The most noticeable difference was observed in the electrical resistivity of vesicular intervals. While Zakharova *et al.* (2012) recorded a narrow variation of electrical resistivity, ranging from 10–20 Ωm, our work found variations between 2.26 and 6,462.78 Ωm, with a median value of 39.27 Ωm. These dissimilarities are probably related to porosity and/or pore fluid characteristics.

The median Vp we identified was 3.9 km/s, significantly below the sonic velocity for flow interior and weathered basalts, but close to the clay lenses value. Zakharova *et al.* (2012) noted that the sonic velocities in vesicular basalt are about 50% of the values found in massive basalt. We found that the median Vp of vesicular and interior flow diverges around 30%. This difference may be attributed to variations of porosity between the massive and vesicular basalts of Serra Geral and Columbia River Basalts.

The vesicular intervals of basalt have high average gamma-ray values of 15.58 API, close to the values in weathered basalt and slightly higher than interior flow. Thus, gamma-rays are not useful to diagnose vesicular basalts. However, amygdaloidal basalts are strongly subjected to weathering due to the reactivity of glassy material and high-porosity, producing

clays. As noted by Buckley and Oliver (1990) in Deccan traps, vesicular basalts may present high gamma-rays whenever there is pronounced weathering.

Weathered basalt

The analysis of drill cutting samples indicated that some intervals possess centimetric rounded and brown fragments, containing vesicles filled with zeolites, carbonates, and chlorite, associated with clay intervals. The development of physical and chemical weathering is likely to be intensive in basalts due to the high reactivity of major minerals in these rocks (olivines, pyroxenes, and plagioclases). Weathering progress increases the aperture of fractures and leachates the silicates, promoting a strong increase in porosity and permeability. The time interval between two lava flow events can play a crucial role in the development of an aquifer zone within the basaltic units. After lava consolidation, chemical and physical weathering take place, creating a weathering profile where permeability and porosity values are especially higher. Both Buckley and Oliver (1990) and Gingerich and Izuka (1997) verified — on the Deccan Plateau, India and in Hawaii, the United States, respectively — the existence of weathered basalt in deep portions overlapped by non-weathered basalts. On the other hand, the core description presented by Zakharova et al. (2012) did not find weathered basalts, indicating that the weathered facies are not widespread in all basalts.

Resistivity is commonly considered the main tool to distinguish low-porosity flow interior and high-porosity flow top, since resistivity is very sensitive to changes in porosity, water-filling pores, and the presence of clay. In response to high-porosity and to the presence of clay minerals, the weathered basalt has an electrical resistivity median of 66 Ωm (Fig. 4B), a value between the flow interiors and the vesicular or clay intervals.

As demonstrated by Navarre-Sitchler et al. (2015), during the chemical weathering of basalt, rock porosity strongly increases. Thus, chemical weathering enables the use of acoustic velocity as an important tool to identify weathered intervals, since the porosity enhancement is diagnosed by the decrease in P wave acoustic velocity. The median Vp of weathered basalt is 4.5 km/s, consistently below the flow interior value (5.6 km/s), and above the sonic velocities of clay and vesicular intervals (4.3 and 3.9 km/s, respectively), as seen in Figure 4C.

Weathered basalts present a mean gamma radiation of 25.64 API, highly divergent from flow interior and vesicular basalts. The increase in gamma radiation may be related to the presence of clay minerals produced by pyroxene and plagioclase weathering. Thus, gamma radiation represents another parameter used to identify weathered basalts due to the abundance of clay minerals.

Clay lenses

Weathered horizons are associated with the presence of thick lenses of clay reported in this study as well as in previous works (e.g., Buckley and Oliver 1990, Gingerich and Izuka 1997, Jalludin and Razack 2004), and are evidence of ancient weathering surface development. Interestingly, clay lenses were not recorded in the Columbia River Basalts (Zakharova et al. 2012).

As stated by Helm-Clark et al. (2004), gamma-ray logs are unfeasible tools to identify anomalous intervals containing high potassium concentrations, which is often related to the presence of clay minerals (mainly smectite) produced by basalt weathering processes. Buckley and Oliver (1990) and Crosby and Anderson (1971) demonstrated the applicability of gamma-ray profiling tools for identification of clay lenses produced by basalt weathering. In the present study, the presence of weathered basalt associated with clay lenses was also easily identified by gamma-ray logs interpretation.

The median resistivity obtained for the clay lenses was 48.35 Ωm, close to vesicular (39.27 Ωm) and weathered (66 Ωm) intervals. The median Vp of clay lenses is 4.3 km/s, below that of vesicular basalts, and very different from weathered basalts and flow interior especially. This signature is compatible with the high-porosity of clay lenses.

Porosity and permeability derived from wireline logs

In order to build an empirical model able to produce reliable estimates of porosity from acoustic velocity, we compiled experimental data from Zamora et al. (1994), Al-Harthi et al. (1999), Planke et al. (1999), Chen et al. (2015), Vedanti et al. (2018), and Rossetti et al. (2019) relating porosity of basalts to sonic velocity (Fig. 5). Using non-linear regression, an exponential equation was fitted to 197 data points of porosity and V_p, including samples spanning from massive to vesicular basalts. Due to sample size, the identified equation from non-linear regression (Eq. 1) is representative of all facies within the basalt flow.

$$\theta = 54.746e^{-0.821\left(V_P - 2.369\right)} \tag{1}$$

The porosity derived from sonic logs represents a quantitative parameter used to determine the permeable and impermeable intervals of basaltic aquifers. The contact between two successive basalt flows is characterized by an abrupt change in porosity, as seen in Figure 6. The recurrent overlap of high- (vesicular, amygdaloidal, and scoria) and low-porosity zones (massive, columnar, and entablature basalts) is evident. We estimated porosity based on Equation 1, building porosity
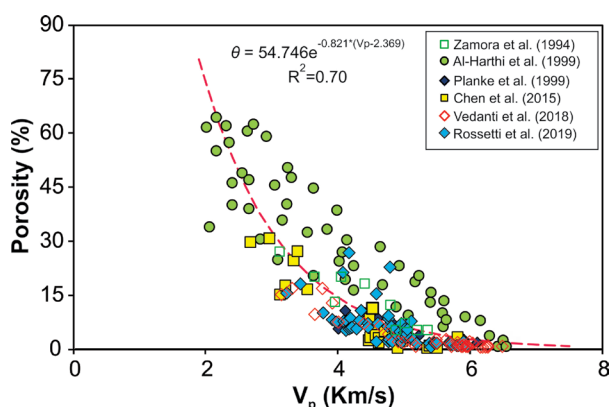

Figure 5. Scatterplot of porosity as a function of V_p and the exponential equation fitted to relate both parameters.

profiles for wells SAG/P2 and SAG/P3. In order to compare with wireline logs from the Columbia Plateau, we also derived porosity using Vp logs presented by Zakharova *et al.* (2012). The porosity profiles of SAG/P2, SAG/P3, and the well from Zharakova *et al.* (2012) are presented in Figure 6.

The porosity profile estimated by Equation 1 (Fig. 6) produces well-delimited intervals of porosity in complete agreement with the limits of basalt hydrofacies. Furthermore, Figure 6 reveals that basalts of the Columbia Plateau and the Serra Geral Aquifer have the same internal structure, displaying alternations of high and low porosity zones as well as a comparable range of porosity values. The main differences are related to the thickness of high porosity zones. While the intervals containing high-porosity in the Columbia Plateau have an average thickness of approximately 8 m, those of Serra Geral Aquifer have a thickness of approximately 12 m, reflecting the volume of lava expelled as well as its temperature and magma composition. The porosity of flow tops (vesicular, breccia, and scoria) represents the primary porosity and is generated by degassing during the cooling of sub-aerial flows, and is dependent on bubble gas and lava flow characteristics (Sahagian *et al.* 1989, Mangan and Cashman 1996, Melnik 2000). Vesicular basalt is characterized by high porosity due to its genetic context. The porosity of vesicular basalt was estimated using Equation 1 as ranging from 20 to 60%, agreeing with experimental results presented by Saar and Manga (1999), Song *et al.* (2001), Shea *et al.* (2010), and Schaefer *et al.* (2015). Reported anomalously high porosity values are associated with scoriaceous rocks, with porosity above 40% (Saar and Manga 1999, Song *et al.* 2001), which were not found on the studied wells.

In general, the porosity of the flow interior is very low (*e.g.*, Christensen and Wilkens 1982, Vinciguerra *et al.* 2005, Zakharova *et al.* 2012). While Vinciguerra *et al.* (2005) reported a porosity of 1% for columnar basalt, Christensen and Wilkens (1982) reported values in the range of 0.1–1.9%. Zakharova *et al.* (2012) verified that flow interiors are characterized by
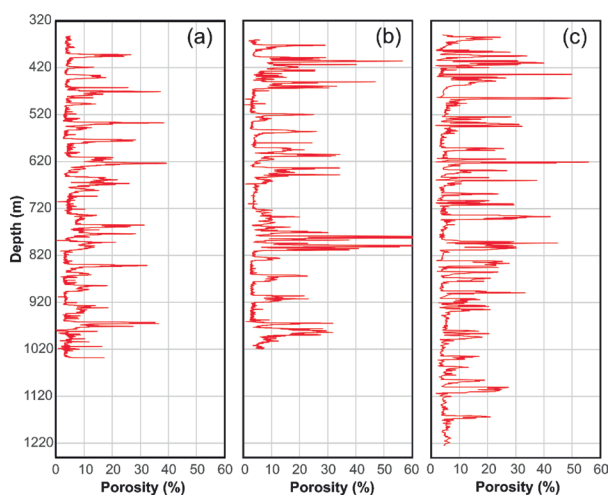
porosity values ranging from 0 to 10%, where higher porosity values (5–10%) correspond to higher planar fracture density. The highest porosity values of flow interiors were reported by Deolankar (1980); 15% were related to fractured basalts. Figure 6 reveals that our model predicted porosities around 4% for massive basalts in the Serra Geral Formation and the Columbia Plateau.

Experimental porosity and permeability data encompass all lithologies found in flood basalts, with porosity ranging from 1.07 to 87% and permeability ranging from 4.34×10^{-18} to 6.89×10^{-11} m². Using non-linear regression, we established a model able to predict the permeability based on porosity data (Eq. 2). The goodness of fit was obtained using the least-squares method of optimizing the Kozeny–Carman model by minimization of the average error (Fig. 7).

$$k = 4 \times 10^{-18} \theta^{3.245} \qquad (2)$$

The scatterplot graph of natural logarithm of predicted permeability by Equation 2 *versus* observed permeability (Fig. 7B) indicates a good agreement of both values, supporting the ability of our model to produce reasonable permeability estimation. The minimum porosity value calculated in basalt was 0%, while the maximum was 39.4%. A rough estimation of permeability can be performed by applying Equation 2 and sonic-derived porosity data (Figs. 8 and 9).

In this study, the ranges of permeability values estimated (Figs. 8 and 9) produce values compatible with those recorded
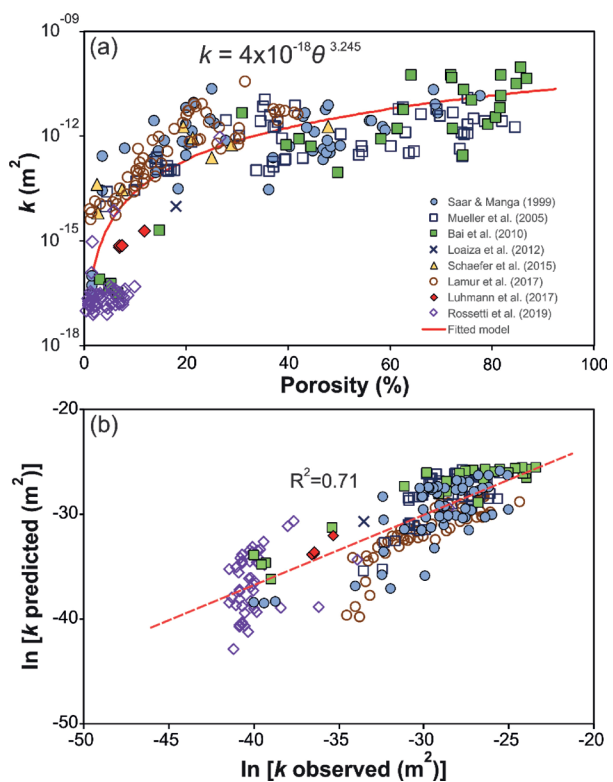

Figure 6. Comparison of sonic-derived porosity from Equation 1 displaying similar patterns, with alternation of high (flow tops) and low (flow interiors) porosity zones. (A) Log profile of SAG/P2; (B) Log profile of SAG/P3; (C) Log profile of Columbia Plateau, presented by Zakharova *et al.* (2012).

Figure 7. Permeability and porosity relation based on data compiled from previous works: (A) The fitted Kozeny-Carman model (curve) was optimized through a nonlinear least square regression; (B) Scatterplot graph of natural logarithm of predicted permeability by fitted model against observed permeability.

in the literature. The reported permeability ranges determined for the flow tops (vesicular, breccia, and scoria) are usually high, with values ranging from 1.7×10^{-15} to 2.4×10^{-12} m^2 (Saar and Manga 1999, McGrail *et al.* 2001, Schaefer *et al.* 2015, Lamur *et al.* 2017). The permeability and porosity of the interior part of basalt flows (massive, colonnade, and entablature) are less commonly studied than those of flow tops. McGrail *et al.* (2011) and Nara *et al.* (2011) determined

the permeability of the flow interior ranging from 10^{-20} to 10^{-19} m^2. According to McGrail *et al.* (2006) and Zakharova *et al.* (2012), the presence of fractures or joints generally does not significantly contribute to the increase in basalt permeability. Figure 10 summarizes the statistics (min, max, mean, and standard deviation) of porosity and permeability estimations produced, respectively, by empirical Equations 1 and 2 for the different basalt hydrofacies.
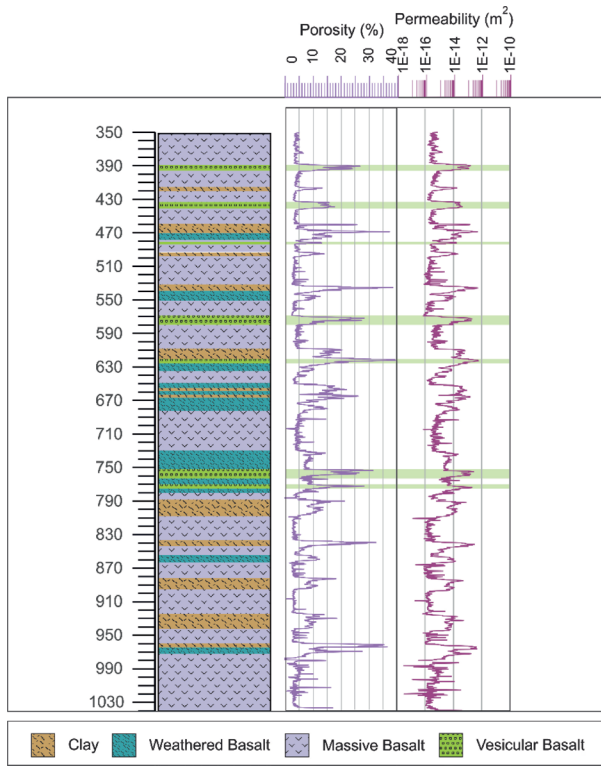

Figure 8. Porosity, permeability and geological profiles of well SAG/P2. The permeability profile of SAG/P2 was estimated using Equation 2 with sonic-derived porosity.
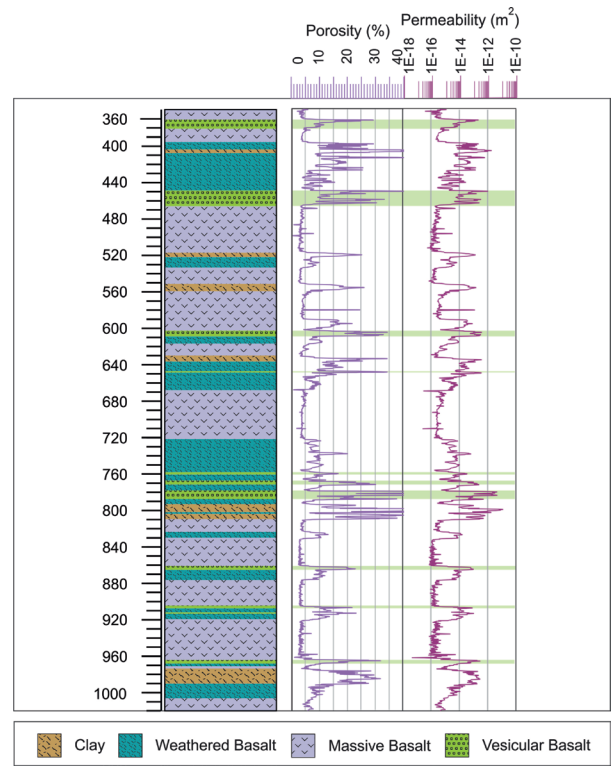

Figure 9. Porosity, permeability and geological profiles of well SAG/P3. The permeability profile of SAG/P3 was estimated using Equation 2 with sonic-derived porosity.
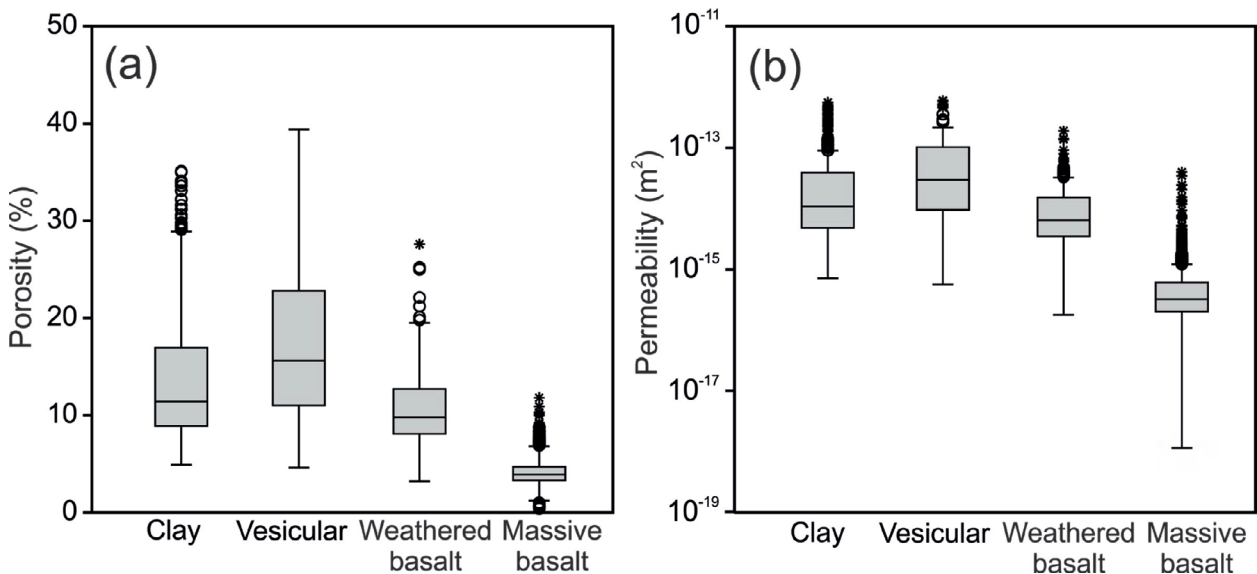

Figure 10. Boxplots showing the distribution of estimated porosity and permeability for the basalt flows intercepted by SAG/P2 and SAG/P3 wells: (A) porosity; (B) permeability. The lower and upper caps at the end of each box indicate respectively the minimum and maximum values, the box limits are delineated by the first and third quartiles, and the line in the center of the box represents the median.

CONCLUSIONS

The wireline logs presented in this study strongly suggest that basalts are best described as multilayered aquifers, in which permeable zones correspond to flow tops (vesicular, breccia, and scoria), that alternate with low permeability intervals represented by flow interiors (massive, columnar, and entablature basalt). Additionally, we recognized the presence of permeable intervals associated with weathered zones and clay lenses produced by intensive basalt weathering. Our analysis reinforces the use of well logs to identify the high and low permeability intervals of basalt flows. The analysis of compiled experimental data allowed us to produce an empirical equation capable to estimate porosity based on acoustic velocity logs. Our analysis also indicates that permeability may be successfully estimated from porosity using the Kozeny-Carman model. Thus, wireline logs provide a reasonable estimation of the hydraulic properties of basaltic aquifers.

ACKOWLEDGMENTS

REFERENCES

Al-Harthi A.A., Al-Amri R.M., Shehata W.M. 1999. The porosity and engineering properties of vesicular basalt in Saudi Arabia. *Engineering Geology*, **54**(3-4):313-320. https://doi.org/10.1016/S0013-7952(99)00050-2

Almeida F.F. 1986. Distribuição regional e relações tectônicas do magmatismo pós-paleozóico no Brasil. *Revista Brasileira de Geociências*, **16**(4):325-349.

Asfahani J. 2011. Basalt characterization by means of nuclear and electrical well logging techniques. Case study from Southern Syria. *Applied Radiation and Isotopes*, **69**(3):641-647. https://doi.org/10.1016/j.apradiso.2010.12.008

Bai L., Baker D.R., Hill R.J. 2010. Permeability of vesicular Stromboli basaltic glass: Lattice Boltzmann simulations and laboratory measurements. *Journal of Geophysical Research: Solid Earth*, **115**(B7). https://doi.org/10.1029/2009jb007047

Barreto C.J.S., Lafon J.M., de Lima E.F., Sommer C.A. 2016. Geochemical and Sr–Nd–Pb isotopic insight into the low-Ti basalts from southern Paraná Igneous Province, Brazil: the role of crustal contamination. *International Geology Review*, **58**(11):1324-1349. https://doi.org/10.1080/00206814.2016.1147988

Browning J., Meredith P., Gudmundsson A. 2016. Cooling-dominated cracking in thermally stressed volcanic rocks. *Geophysical Research Letters*, **43**(16):8417-8425. https://doi.org/10.1002/2016gl070532

Buckley D.K., Oliver D. 1990. Geophysical logging of water exploration boreholes in the Deccan Traps, Central India. *Geological Society, London, Special Publications*, **48**(1):153-161. https://doi.org/10.1144/GSL.SP.1990.048.01.13

Cabrera M.C., Custodio E. 2004. Groundwater flow in a volcanic–sedimentary coastal aquifer: Telde area, Gran Canaria, Canary Islands, Spain. *Hydrogeology Journal*, **12**:305-320. https://doi.org/10.1007/s10040-003-0316-y

Chen X., Schmitt D.R., Kessler J.A., Evans J., Kofman R. 2015. Empirical relations between ultrasonic P-wave velocity porosity and uniaxial compressive strength. *CSEG Rec*, **40**(5):24-29.

Christensen N.I., Wilkens R.H. 1982. Seismic properties, density, and composition of the Icelandic crust near Reydarfjördur. *Journal of Geophysical Research: Solid Earth*, **87**(B8):6389-6395. https://doi.org/10.1029/JB087iB08p06389

Crosby III J.W., Anderson J.V. 1971. Some applications of geophysical well logging to basalt hydrogeology. *Groundwater*, **9**(5):12-20. https://doi.org/10.1111/j.1745-6584.1971.tb03562.x

Degruyter W., Bachmann O., Burgisser A. 2010. Controls on magma permeability in the volcanic conduit during the climactic phase of the Kos Plateau Tuff eruption (Aegean Arc). *Bulletin of Volcanology*, **72**. https://doi.org/10.1007/s00445-009-0302-x

Deolankar S.B. 1980. The Deccan basalts of Maharashtra, India—their potential as aquifers. *Groundwater*, **18**(5):434-437. https://doi.org/10.1111/j.1745-6584.1980.tb03416.x

Edmunds W.M., Carrillo-Rivera J.J., Cardona A. 2002. Geochemical evolution of groundwater beneath Mexico City. *Journal of Hydrology*, **258**(1-4):1-24. https://doi.org/10.1016/S0022-1694(01)00461-9

El-Kadi A.I., Tillery S., Whittier R.B., Hagedorn B., Mair A., Ha K., Koh G.W. 2014. Assessing sustainability of groundwater resources on Jeju Island, South Korea, under climate change, drought, and increased usage. *Hydrogeology Journal*, **22**:625-642. https://doi.org/10.1016/j.geomorph.2009.01.009

Farquharson J., Heap M.J., Varley N.R., Baud P., Reuschlé T. 2015. Permeability and porosity relationships of edifice-forming andesites: a combined field and laboratory study. *Journal of Volcanology and Geothermal Research*, **297**:52-68. https://doi.org/10.1016/j.jvolgeores.2015.03.016

Frank H.T., Gomes M.E.B., Formoso M.L.L. 2009. Review of the areal extent and the volume of the Serra Geral Formation, Paraná Basin, South America. *Pesquisas em Geociências*, **36**(1):49-57.

Gingerich S.B., Izuka S.K. 1997. *Construction, geologic log, and aquifer test of the Northwest Kilohana Monitor Well (State well 2-0126-01)*. Lihue, Kauai, Hawaii: US Geological Survey Open-File Report, p. 97-40.

Helm-Clark C.M., Rodgers D.W., Smith R.P. 2004. Borehole geophysical techniques to define stratigraphy, alteration and aquifers in basalt. *Journal of Applied Geophysics*, **55**(1-2):3-38. http://doi.org/10.1016/j.jappgeo.2003.06.003

Jalludin M., Razack M. 2004. Assessment of hydraulic properties of sedimentary and volcanic aquifer systems under arid conditions in the Republic of Djibouti (Horn of Africa). *Hydrogeology Journal*, **12**:159-170. http://doi.org/10.1007/s10040-003-0312-2

James A.V. 1920. Factors producing columnar structure in lavas and its occurrence near Melbourne, Australia. *The Journal of Geology*, **28**(5):458-469. https://doi.org/10.1086/622727

Kattenhorn S.A., Schaefer C.J. 2008. Thermal–mechanical modeling of cooling history and fracture development in inflationary basalt lava flows. *Journal of Volcanology and Geothermal Research*, **170**(3-4):181-197. http://doi.org/10.1016/j.jvolgeores.2007.10.002

Klug C., Cashman K.V. 1996. Permeability development in vesiculating magmas: implications for fragmentation. *Bulletin of Volcanology*, **58**:87-100. http://doi.org/10.1007/s004450050128

Kulkarni H., Deolankar S.B., Lalwani A., Joseph B., Pawar S. 2000. Hydrogeological framework of the Deccan basalt groundwater systems, west-central India. *Hydrogeology Journal*, **8**:368-378. http://doi.org/10.1007/s100400000079

Lamur A., Kendrick J.E., Eggertsson G.H., Wall R.J., Ashworth J.D., Lavallée Y. 2017. The permeability of fractured rocks in pressurised volcanic and geothermal systems. *Scientific Reports*, **7**:6173. http://doi.org/10.1038/s41598-017-05460-4

Limaye S.D. 2010. Groundwater development and management in the Deccan Traps (basalts) of western India. *Hydrogeology Journal*, **18**:543-558. http://doi.org/10.1007/s10040-009-0566-4

Loaiza S., Fortin J., Schubnel A., Gueguen Y., Vinciguerra S., Moreira M. 2012. Mechanical behavior and localized failure modes in a porous basalt from the Azores. *Geophysical Research Letters*, **39**(19). http://doi.org/10.1029/2012GL053218

Locsey K.L., Cox M.E. 2003. Statistical and hydrochemical methods to compare basalt-and basement rock-hosted groundwaters: Atherton Tablelands, north-eastern Australia. *Environmental Geology*, **43**:698-713. http://doi.org/10.1007/s00254-002-0667-z

Long P.E., Wood B.J. 1986. Structures, textures, and cooling histories of Columbia River basalt flows. *Geological Society of America Bulletin*, **97**(9):1144-1155. https://doi.org/10.1130/0016-7606(1986)97%3C1144:STACHO%3E2.0.CO;2

Lore J., Gao H., Aydin A. 2000. Viscoelastic thermal stress in cooling basalt flows. *Journal of Geophysical Research: Solid Earth*, **105**(B10):23695-23709. https://doi.org/10.1029/2000JB900226

Luhmann A.J., Tutolo B.M., Bagley B.C., Mildner D.F., Seyfried Jr. W.E., Saar M.O. 2017. Permeability, porosity, and mineral surface area changes in basalt cores induced by reactive transport of CO_2-rich brine. *Water Resources Research*, **53**(3):1908-1927. https://doi.org/10.1002/2016WR019216

Machado F.B., Reis Viana Rocha-Júnior E., Soares Marques L., Ranalli Nardy A.J. 2015. Volcanological aspects of the northwest region of Paraná continental flood basalts (Brazil). *Solid Earth*, **6**(1):227-241.

Mangan M.T., Cashman K.V. 1996. The structure of basaltic scoria and reticulite and inferences for vesiculation, foam formation, and fragmentation in lava fountains. *Journal of Volcanology and Geothermal Research*, **73**(1-2):1-18. https://doi.org/10.1016/0377-0273(96)00018-2

McGrail B.P., Schaef H.T., Ho A.M., Chien Y.J., Dooley J.J., Davidson C.L. 2006. Potential for carbon dioxide sequestration in flood basalts. *Journal of Geophysical Research: Solid Earth*, **111**(B12). https://doi.org/10.1029/2005JB004169

McGrail B.P., Spane F.A., Sullivan E.C., Bacon D.H., Hund G. 2011. The Wallula basalt sequestration pilot project. *Energy Procedia*, **4**:5653-5660. https://doi.org/10.1016/j.egypro.2011.02.557

McKenzie J.M., Siegel D.I., Patterson W., McKenzie D.J. 2001. A geochemical survey of spring water from the main Ethiopian rift valley, southern Ethiopia: implications for well-head protection. *Hydrogeology Journal*, **9**:265-272. https://doi.org/10.1007/s100400100134

Melnik O. 2000. Dynamics of two-phase conduit flow of high-viscosity gas-saturated magma: large variations of sustained explosive eruption intensity. *Bulletin of Volcanology*, **62**:153-170. https://doi.org/10.1007/s004450000072

Mueller S., Melnik O., Spieler O., Scheu B., Dingwell D.B. 2005. Permeability and degassing of dome lavas undergoing rapid decompression: an experimental determination. *Bulletin of Volcanology*, **67**(6):526-538. https://doi.org/10.1007/s00445-004-0392-4

Nara Y., Meredith P.G., Yoneda T., Kaneko K. 2011. Influence of macro-fractures and micro-fractures on permeability and elastic wave velocities in basalt at elevated pressure. *Tectonophysics*, **503**(1-2):52-59. https://doi.org/10.1016/j.tecto.2010.09.027

Navarre-Sitchler A., Brantley S.L., Rother G. 2015. How porosity increases during incipient weathering of crystalline silicate rocks. *Reviews in Mineralogy and Geochemistry*, **80**(1):331-354. https://doi.org/10.2138/rmg.2015.80.10

Peterson F.L., Lao C. 1970. Electric well logging of Hawaiian basaltic aquifers. *Groundwater*, **8**(2):11-18. https://doi.org/10.1111/j.1745-6584.1970.tb01674.x

Piersol M.W., Sprenke K.F. 2015. A Columbia River Basalt Group Aquifer in Sustained Drought: Insight from Geophysical Methods. *Resources*, **4**(3):577-596. https://doi.org/10.3390/resources4030577

Planke S., Cerney B., Bücker C.J., Nilsen O. 1999. Alteration effects on petrophysical properties of subaerial flood basalts: Site 990, Southeast Greenland margin. *In*: *Proceedings of the Ocean Drilling Program Scientific Results*, v. 163, p. 17-28. Ocean Drilling Program College Station, TX. https://doi.org/10.2973/odp.proc.ir.163.1996

Polo L.A., Janasi V.A., Giordano D., Lima E.F., Cañon-Tapia E., Roverato M. 2018. Effusive silicic volcanism in the Paraná Magmatic Province, South Brazil: Evidence for locally-fed lava flows and domes from detailed field work. *Journal of Volcanology and Geothermal Research*, **355**:204-218. https://doi.org/10.1016/j.jvolgeores.2017.08.007

Prada S.N., Silva M.O., Cruz J.V. 2005. Groundwater behaviour in Madeira, volcanic island (Portugal). *Hydrogeology Journal*, **13**(5-6):800-812. https://doi.org/10.1007/s10040-005-0448-3

Puffer J.H., Block K.A., Steiner J.C., Laskowich C. 2018. Complex layering of the Orange Mountain Basalt: New Jersey, USA. *Bulletin of Volcanology*, **80**(6):54. https://doi.org/10.1093/petrology/egt063

Raymer L.L., Hunt E.R., Gardner J.S. 1980. An improved sonic transit time-to-porosity transform. *In*: SPWLA 21st Annual Logging Symposium. *Proceedings…* Society of Petrophysicists and Well-Log Analysts.

Rossetti L., Lima E.F., Waichel B.L., Hole M.J., Simões M.S., Scherer C.M. 2018. Lithostratigraphy and volcanology of the Serra Geral Group, Paraná-Etendeka Igneous Province in southern Brazil: Towards a formal stratigraphical framework. Journal of Volcanology and Geothermal Research, **355**:98-114. https://doi.org/10.1016/j.jvolgeores.2017.05.008

Rossetti L.M., Healy D., Hole M.J., Millett J.M., de Lima E.F., Jerram D.A., Rossetti M.M.M. 2019. Evaluating petrophysical properties of volcano-sedimentary sequences: A case study in the Paraná-Etendeka Large Igneous Province. *Marine and Petroleum Geology*, **102**:638-656. https://doi.org/10.1016/j.marpetgeo.2019.01.028

Saar M.O., Manga M. 1999. Permeability-porosity relationship in vesicular basalts. *Geophysical Research Letters*, **26**(1):111-114. https://doi.org/10.1016/j.jvolgeores.2017.05.008

Sahagian D.L., Anderson A.T., Ward B. 1989. Bubble coalescence in basalt flows: comparison of a numerical model with natural examples. *Bulletin of Volcanology*, **52**(1):49-56. https://doi.org/10.1007/BF00641386

Schaefer L.N., Kendrick J.E., Oommen T., Lavallée Y., Chigna G. 2015. Geomechanical rock properties of a basaltic volcano. *Frontiers in Earth Science*, **3**:29. https://doi.org/10.3389/feart.2015.00029

Schlumberger Wireline and Testing. 1989. *Log Interpretation Principles/Applications Sugarland*. Texas, Schlumberger Wireline and Testing, 251 p.

Shea T., Houghton B.F., Gurioli L., Cashman K.V., Hammer J.E., Hobden B.J. 2010. Textural studies of vesicles in volcanic rocks: an integrated methodology. *Journal of Volcanology and Geothermal Research*, **190**(3-4):271-289. https://doi.org/10.1016/j.jvolgeores.2009.12.003

Song S.R., Jones K.W., Lindquist B.W., Dowd B.A., Sahagian D.L. 2001. Synchrotron X-ray computed microtomography: studies on vesiculated basaltic rocks. *Bulletin of Volcanology*, **63**(4):252-263. https://doi.org/10.1007/s004450100141

Svensen H.H., Torsvik T.H., Callegaro S., Augland L., Heimdal T.H., Jerram D.A., Planke S., Pereira E. 2017. Gondwana Large Igneous Provinces: plate reconstructions, volcanic basins and sill volumes. *Geological Society, London, Special Publications*, **463**(1):17-40. https://doi.org/10.1144/SP463.7

Takeuchi S., Nakashima S., Tomiya A. 2008. Permeability measurements of natural and experimental volcanic materials with a simple permeameter: toward an understanding of magmatic degassing processes. *Journal of Volcanology and Geothermal Research*, **177**(2):329-339. https://doi.org/10.1016/j.jvolgeores.2008.05.010

Tomkeieff S.I. 1940. The basalt lavas of the Giant's Causeway district of Northern Ireland. *Bulletin of Volcanology*, **6**:89-143. https://doi.org/10.1007/BF02994875

Turner S., Regelous M., Kelley S., Hawkesworth C., Mantovani M. 1994. Magmatism and continental break-up in the South Atlantic: high precision40Ar-39Ar geochronology. *Earth and Planetary Science Letters*, **121**(3-4):333-348. https://doi.org/10.1016/0012-821X(94)90076-0

Uhl Jr. V.W., Joshi V.G. 1986. Results of pumping tests in the Deccan trap basalts of central India. *Journal of Hydrology*, **86**(1-2):147-168. https://doi.org/10.1016/0022-1694(86)90011-9

Vedanti N., Malkoti A., Pandey O.P., Shrivastava J.P. 2018. Ultrasonic P-and S-Wave Attenuation and Petrophysical Properties of Deccan Flood Basalts, India, as Revealed by Borehole Studies. *Pure and Applied Geophysics*, **175**(8):2905-2930. https://doi.org/10.1007/s00024-018-1817-x

Vinciguerra S., Trovato C., Meredith P.G., Benson P.M. 2005. Relating seismic velocities, thermal cracking and permeability in Mt. Etna and Iceland basalts. *International Journal of Rock Mechanics and Mining Sciences*, **42**(7-8):900-910. https://doi.org/10.1016/j.ijrmms.2005.05.022

Walker G.P.L. 1971. Compound and simple lava flows and flood basalts. *Bull Volcanology*, **35**:579-590. https://doi.org/10.1007/BF02596829

Wentworth C.K. 1951. *Geology and ground-water resources of the Honolulu-Pearl Harbor area Oahu, Hawaii*. Honolulu: Honolulu Board of Water Supply, 111 p.

Whitehead R.L. 1992. *Geohydrologic framework of the Snake River Plain regional aquifer system, Idaho and eastern Oregon*. No. 1408-B. US Government Printing Office. https://doi.org/10.3133/pp1408b

Wyllie M.R.J., Gregory A.R., Gardner L.W. 1956. Elastic Wave Velocities in Heterogeneous and Porous Media. *Geophysics*, **21**(1):41-70. http://dx.doi.org/10.1190/1.1438217

Yokoyama T., Takeuchi S. 2009. Porosimetry of vesicular volcanic products by a water-expulsion method and the relationship of pore characteristics to permeability. *Journal of Geophysical Research: Solid Earth*, **114**(B2). https://doi.org/10.1029/2008JB005758

Zakharova N.V., Goldberg D.S., Sullivan E.C., Herron M.M., Grau J.A. 2012. Petrophysical and geochemical properties of Columbia River flood basalt: Implications for carbon sequestration. *Geochemistry, Geophysics, Geosystems*, **13**(11). https://doi.org/10.1029/2012gc004305

Zamora M., Sartoris G., Chelini W. 1994. Laboratory measurements of ultrasonic wave velocities in rocks from the Campi Flegrei volcanic system and their relation to other field data. *Journal of Geophysical Research: Solid Earth*, **99**(B7):13553-13561. https://doi.org/10.1029/94jb0012